INL/CON-15-34140-Revision-0

SENSITIVITY EVALUATION OF THE DAILY THERMAL PREDICTIONS OF THE AGR-2 EXPERIMENT IN THE ADVANCED TEST REACTOR

Grant Hawkes, Jim Sterbentz, Binh Pham

June 2015

The INL is a U.S. Department of Energy National Laboratory
operated by Battelle Energy Alliance

INL/CON-15-34140-Revision-0

SENSITIVITY EVALUATION OF THE DAILY THERMAL PREDICTIONS OF THE AGR-2 EXPERIMENT IN THE ADVANCED TEST REACTOR

Grant Hawkes, Jim Sterbentz, Binh Pham

June 2015

Idaho National Laboratory
Idaho Falls, Idaho 83415

http://www.inl.gov

Prepared for the
U.S. Department of Energy

Under DOE Idaho Operations Office
Contract DE-AC07-05ID14517

SENSITIVITY EVALUATION OF THE DAILY THERMAL PREDICTIONS OF THE AGR-2 EXPERIMENT IN THE ADVANCED TEST REACTOR

Grant L. Hawkes
Idaho National Laboratory
Idaho Falls, Idaho, USA

James W. Sterbentz
Idaho National Laboratory
Idaho Falls, Idaho, USA

Binh T. Pham
Idaho National Laboratory
Idaho Falls, Idaho, USA

ABSTRACT

A temperature sensitivity evaluation has been performed for an individual test capsule in the AGR-2 TRISO particle fuel experiment. The AGR-2 experiment is the second in a series of fueled test experiments for TRISO coated fuel particles run in the Advanced Test Reactor at the Idaho National Laboratory. A series of cases were compared to a base case by varying different input parameters in an ABAQUS finite element thermal model. Most input parameters were varied by ±10%, with one parameter ±20%, to show the temperature sensitivity to each parameter. The most sensitive parameters were the outer control gap distance, heat rate in the fuel compacts, and neon gas fraction. The thermal conductivity of the fuel compacts and thermal conductivity of the graphite holder were of moderate sensitivity. The least sensitive parameters were the emissivities of the stainless steel and graphite, along with gamma heat rate in the non-fueled components. Sensitivity calculations were also performed for the fast neutron fluence, which showed a general, but minimal, temperature rise with increasing fluence.

INTRODUCTION

A sensitivity evaluation has been performed for the daily thermal analyses performed on the advanced gas-cooled reactor (AGR) experiment (AGR-2) in the Advanced Test Reactor (ATR). Six capsules were separately analyzed for each day of the experiment as discussed in [1]. This paper discusses the sensitivity to various input parameters for one capsule (Capsule 5) at one point in time during the irradiation. Twenty seven different runs were performed for this sensitivity analysis.

Several fuel and material irradiation experiments, which support the development of the Next Generation Nuclear Plant (NGNP), are planned for the AGR Fuel Development and Qualification Program. The goals of these experiments are to (a) provide irradiation performance data to support fuel process development, (b) qualify fuel for normal operating conditions, (c) support development and validation of fuel performance and fission product transport models and codes, and (d) provide irradiated fuel and materials for post-irradiation examination (PIE) and safety testing. AGR-2 is the second in this series of planned experiments to test tri-structural-isotropic (TRISO) particle-containing fuel compacts, low enriched uranium oxycarbide fuel.

The AGR-2 experiment is comprised of six individual test capsules, approximately 0.034925 m (1.375-in.) in diameter by 0.1524 m (6-in.) long, stacked on top of each other to form the test train. Each capsule contains 12 fuel compacts that are approximately 0.0127 m (0.5-in.) in diameter by 0.0254 m (1-in.) tall. The compacts are composed of fuel particles bound together by a carbon matrix. Each compact contains approximately 4,150 fissile particles (35 vol% particle packing fraction). Each capsule is supplied with a flowing helium/neon gas mixture to control the test temperature and sweep any fission gases that are released to the fission product monitoring system. Temperature control is accomplished by adjusting the gas mixture ratio of the two gases (helium and neon) with differing thermal conductivities.

The general purpose finite element code ABAQUS [2] was used to perform the thermal analysis.

The AGR-2 experiment was placed in the B-12 position in the ATR core as shown in Figure 1. Each capsule contains a graphite holder with three equally spaced fuel compact holder openings as shown in Figure 2. Each holder opening accommodates four axially stacked fuel compacts. Thus, each capsule has three stacks by four fuel compacts per stack for a total of 12 fuel compacts per capsule, with the entire AGR 2 experiment capsule assembly having six capsules by 12 fuel compacts per capsule for a total of 72 fuel compacts.

Figure 3 shows an axial cut view of a typical capsule. The axial arrangement for Stack-1 for all six capsules is also shown. The ABAQUS model has a direct volume-for-volume correlation with the physics model discussed in Reference [4] for the heating of the compacts (each compact is evenly divided axially into two equal parts).

NUMERICAL MODEL AND DISCUSSION

Figures 4 through 9 are used in the description of the model. The finite element mesh is discussed first, followed by a description of the material properties, and ending with the volumetric heat rates imposed on the model.

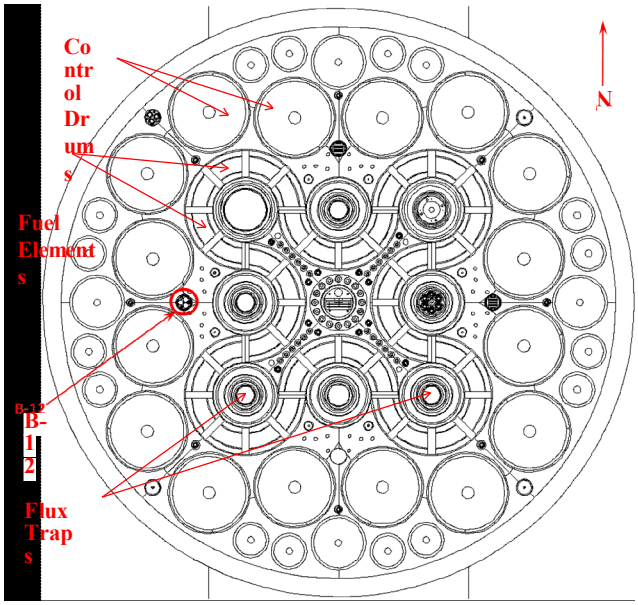

Figure 1. Cross section view of the ATR core, B-12 irradiation test position.

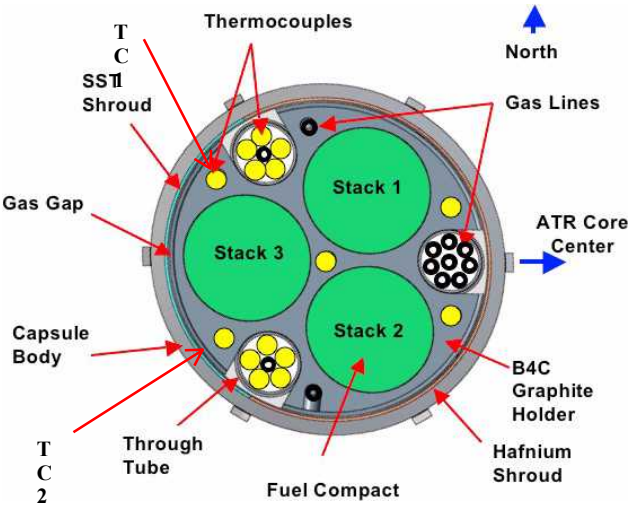

Figure 2. Schematic of cross section of an AGR-2 capsule.

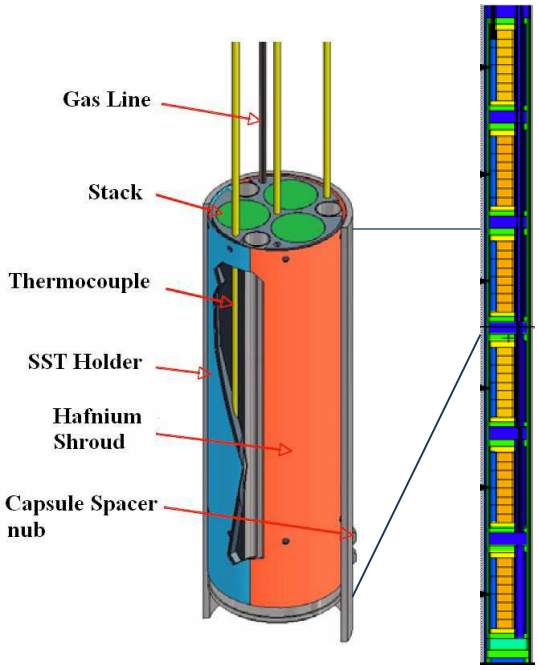

Figure 3. Axial cross-section view of the six capsules in an AGR-2 experiment capsule assembly.

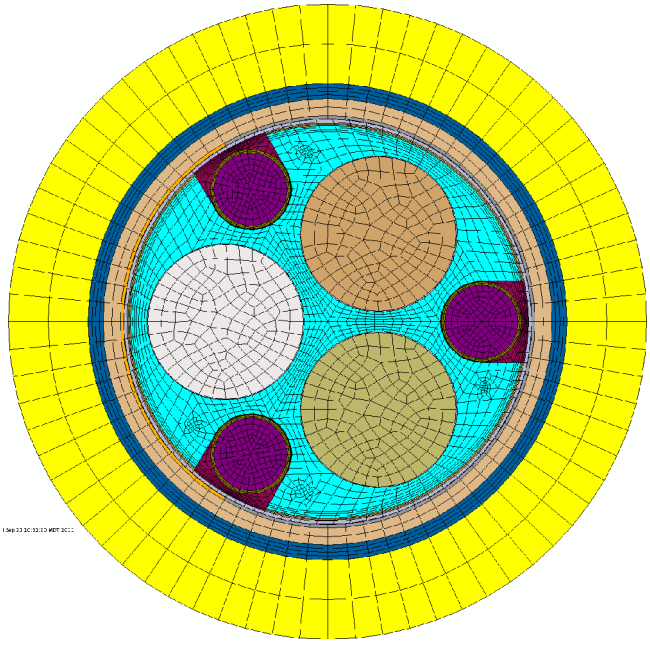

Figure 4. End view finite element mesh.

The finite element mesh is displayed in Figures 4 and 5. Shown in Figure 4 is the cross-sectional end view of the mesh color coded by different entities. Figure 5 shows the finite element mesh with a cutaway view of the entire model. Approximately 350,000 eight-noded hexahedral brick elements were used in all the models. This corresponds to a radial mesh density of 39 elements over

11/16th of an inch, or 57 elements per inch. Several mesh sensitivity studies were performed using this finite element mesh. Results are identical with double, and half the mesh density used in this analysis. This indicates that this sensitivity study is solely a study based on the parameters that are changed and not the variations due to uncertainty in the finite element mesh. A set of conduction-convection elements was used to model the flow of the water. All other elements were modeled solely for diffusion heat transfer.

The graphite holder and fuel compacts were modeled as 0.1016 m (4.0 in.) lengths, but most of the heat comes from the fuel compacts and not from the outer components. The water is the ultimate heat sink for each capsule. The graphite holder with its two end-cap spacers and ring were modeled for the inner part of the model.

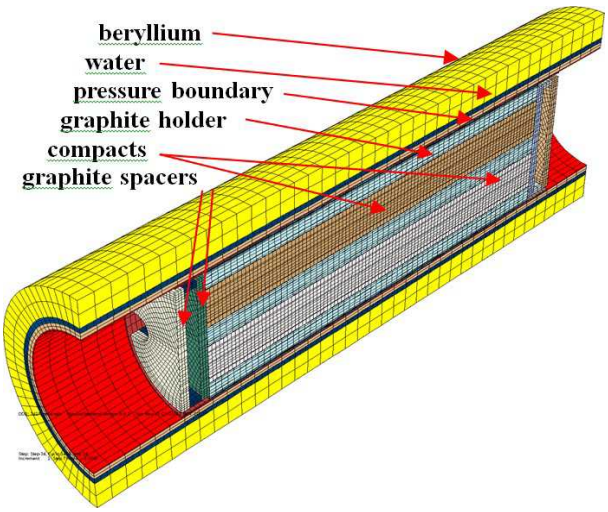

Figure 5. Sideways cutaway view of mesh with colored entities.

The fuel compact thermal conductivity was taken from correlations presented from Gontard in [3] which gives correlations for conductivity, taking into account temperature, temperature of heat treatment, neutron fluence, and TRISO-coated particle packing fraction. In this work, the convention used to quantify neutron damage to a material is fast fluence E >0.18 MeV, yet in the work by [3], the unit used was the dido nickel equivalent (DNE). In order to convert from the DNE convention to the fast fluence >0.18 MeV, the following conversion was used:

$$\Gamma_{>0.18MeV} = 1.52\ \Gamma_{DNE} \quad (1)$$

where Γ is neutron fluence in either the >0.18 MeV unit or DNE. The correlations were developed for a fuel compact matrix density of 1.75 g/cm3, whereas the compact matrix used in AGR-2 had a density of approximately 1.6 and 1.68 g/cm^3 for UCO and UO2 compacts, respectively. The thermal conductivities were scaled according to the ratio of densities (0.91 for UCO and 0.96 for UO2) in order to correct for this difference.

Figure 6 shows a three-dimensional plot of the fuel compact thermal conductivity varying with fluence and temperature for UCO compacts. For fluences greater than 1.0×10^{25} neutrons/m^2 (E > 0.18 MeV), the conductivity increases as fluence increases for higher temperatures, while the opposite occurs at lower temperatures because of the annealing of radiation-induced defects in the material with high temperatures. Figure 7 shows a two-dimensional rendering of the same data from Figure 6 with thermal conductivity varying with fluence with constant values of temperature.

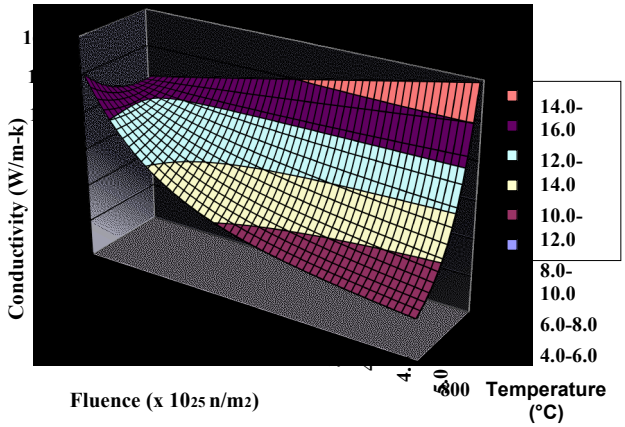

Figure 6. UCO fuel compact thermal conductivity rendition in 3-D.

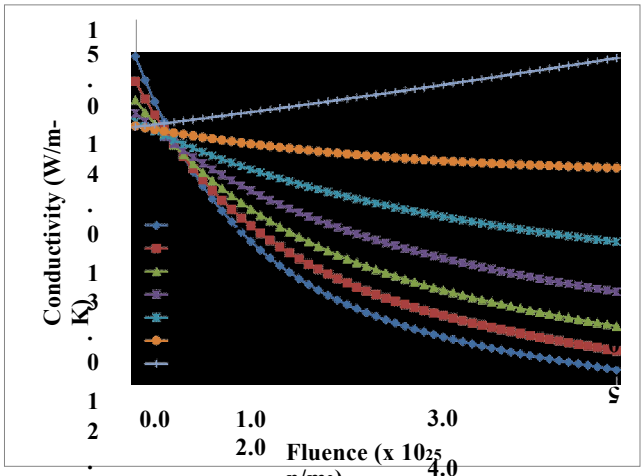

Figure 7. UCO fuel compact thermal conductivity .

Unirradiated graphite thermal conductivity data for the holders were provided by GrafTech [4]. Table 1 shows the unirradiated thermal conductivity for borated graphite ("against grain"). The B4C weight percentage was 4.25%. The boron allowed a more uniform fuel compact fission rate during the irradiation.

Table 1. Thermal conductivity of unirradiated 4.5% borated graphite

Temperature (°C)	Conductivity (W/m-K)
200.0	76.3
300.0	73.4
500.0	60.8
700.0	47.7
900.0	42.7

The effect of irradiation on the thermal conductivity of the graphite was accounted for in this analysis using the following correlation by Snead [5]:

$$\frac{k_{irr}}{k_0} = (0.25 - 0.00017 * T_{irr}) * A * \log(dpa) + 0.000683 * T_{irr}$$
$$A = -1.0 \qquad (2)$$

where k_{irr} and k_0 are thermal conductivity of unirradiated and irradiated graphite, respectively, T_{irr} is the irradiation temperature (°C), and dpa is displacements per atom. The multiplier used to convert fast fluence (>0.18 MeV) to dpa is 8.23 x 10^{-26} dpa/(n/m^2) and comes from Sterbentz [6]. Figure 8 shows a three-dimensional plot of this ratio (k_{irr}/k_o) varying with dpa and temperature. The ratio of unirradiated to irradiated thermal conductivity increases for higher temperatures and decreases for higher dpa.

Heat produced in the fuel compacts is transferred through the gas gaps surrounding the compacts into the graphite holder via a gap conductance model using the gap width and the conductivity of the sweep gas as discussed below. Since the temperature difference between the compacts and the holder is so small, no radiative heat transfer was considered across this gap. Heat is transferred across the outer sweep gas flow region between the outside of the graphite holder and the inside of the stainless-steel liner via radiation between the two surfaces and conduction through the helium/neon sweep gas. Because the thermal capacitance of the sweep gas is very low (30 cc/min), advection is not considered in the sweep gas, and it is modeled as stationary.

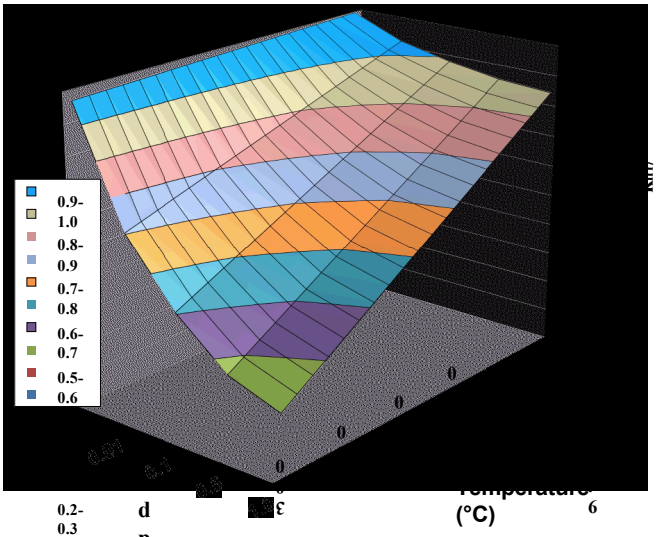

Figure 8. Graphite thermal conductivity plot of ratio of irradiated over unirradiated (k_{irr}/k_o) varying with temperature and dpa.

The thermal conductivity of the sweep gas was determined using the kinetic theory of gases used by the commercial Computational Fluid Dynamics code FLUENT [7], which gives conductivity k of a gas mixture as a function of the gas constituents i and j according to

$$k = \sum_i \frac{Y_i k_i}{\sum_j Y_j \phi_{ij}} \qquad (3)$$

where Y_i is the mole fraction of gas i, and k_i is the thermal conductivity of pure gas i. The parameter ϕ_{ij} in Equation 3 is given by

$$\phi_{ij} = \frac{\left[1 + \left(\frac{\mu_i}{\mu_j}\right)^{1/2} \left(\frac{MW_j}{MW_i}\right)^{1/4}\right]^2}{\left[8\left(1 + \frac{MW_i}{MW_j}\right)\right]^{1/2}} \qquad (4)$$

where μ_i is the viscosity of pure gas i and $M_{w,i}$ is the molecular weight of pure gas i. Pure gas properties were taken from [8]. Figure 9 shows a plot of the resulting helium/neon sweep gas thermal conductivity versus temperature and mole fraction of helium. The thermal conductivity increases as the helium mole fraction increases and as the temperature increases.

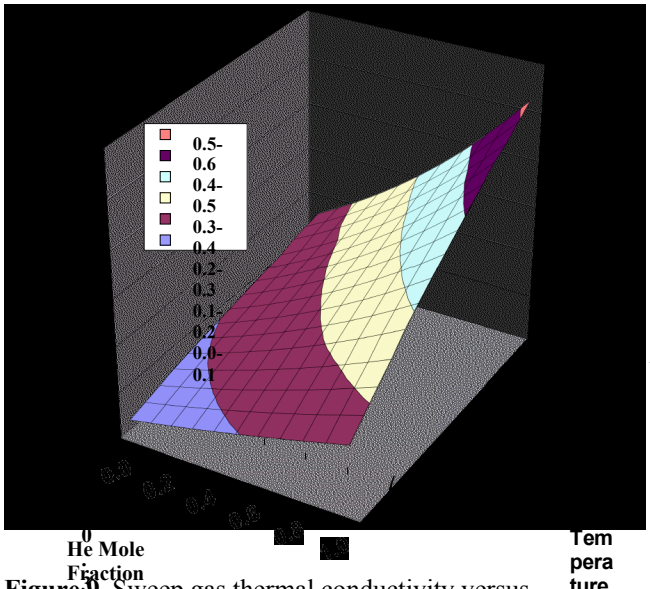

Figure 9. Sweep gas thermal conductivity versus temperature and mole fraction helium.

The governing equation of steady-state heat transfer for the model is taken as

$$\rho c_p \left(u_x \frac{\partial T}{\partial x} + u_y \frac{\partial T}{\partial y} + u_z \frac{\partial T}{\partial z} \right) = \frac{\partial}{\partial x}\left(k(T) \frac{\partial T}{\partial x} \right) + \frac{\partial}{\partial y}\left(k(T) \frac{\partial T}{\partial y} \right) + \frac{\partial}{\partial z}\left(k(T) \frac{\partial T}{\partial z} \right) + Q \quad (5)$$

where ρ is the density, c_p is the specific heat, u_x, u_y, and u_z are the three directional velocities, T is temperature, x, y, and z are directions, $k(T)$ is the thermal conductivity varying with temperature, and Q is the heat source. The velocity of the water (u_z) was taken from Reference [1]. The gas gaps between the graphite holder and the stainless-steel-retainer sleeve used the above mentioned gas mixture conductivity correlation and were modeled with solid eight-noded brick elements with diffusion heat transfer.

Conduction heat transfer across gas gaps using the ABAQUS *Gap Conductance model was implemented on the gaps between surface pairs.

The governing equation for radiation heat transfer across the gas gaps is taken as

$$q_{net} = \frac{\sigma\left(T_1^4 - T_2^4\right)}{\frac{1-\varepsilon_1}{\varepsilon_1 A_1} + \frac{1}{A_1 F_{12}} + \frac{1-\varepsilon_2}{\varepsilon_2 A_2}} \quad (6)$$

where q is the net heat flux, σ is the Stephan Boltzmann constant, T_1 and T_2 are the surface temperatures, ε_1 and ε_2 are the emissivities of surfaces 1 and 2, A_1 and A_2 are the areas of surfaces 1 and 2, and F_{12} is the view factor from surface 1 to 2.

A surface radiation boundary condition using the ABAQUS *Surface Radiation model was placed on the top of the top graphite spacer and the bottom of the bottom graphite spacer and radiated to an infinite medium of (204.4°C) as discussed in [1]. An emissivity value of 1.0 was used for all surfaces. Stainless steel usually has a value around 0.4, but 1.0 was used since a black substance was found on stainless steel during previous AGR experiments [1].

The base case has a gas mixture with 69% neon. Graphite and fuel compact material properties vary with fluence. This was taken as Field Variable 2 in the ABAQUS input model, while the neon fraction was taken as Field Variable 1. Base case fast neutron fluence values are 0.23 x 10^{25} n/m^2. Fast neutron fluence was input for each compact and the graphite holder.

The gamma heating for the various components (not including the fuel compacts) were taken from Reference [9]. These heat rates and fast neutron fluence values were taken from day 43 of the first ATR cycle. This day was selected as a typical day near the beginning of irradiation. Fluence effects would be noticeable, but not dominant. The water heat rate and the beryllium heat rate were included. These rates raise the water temperature as it flows by the capsule, but represent only a small fraction of the total heat. The components on the inside of the water had the greatest effect on the temperature of the fuel compacts and thermocouple locations. All of the internal components in the model use gamma heating rates calculated from [9].

The ABAQUS model and the MCNP model used to do the physics calculations use the exact same volumes for the fuel compacts. The heating volumes in ABAQUS were described with element groups matching one-half of each compact split at the mid-point from top to bottom. These one-half fuel compact heat rates were input into the ABAQUS input file.

Fuel compact heat rates vary by axial position and stack. Actual values for day 43 were used for the base case and ratioed in cases where fuel heat rates were varied. Table 2 shows the base case heat rates for capsule 5 in W/cm^3. The highest heat rates are at the bottom of each stack in capsule 5. The top of each stack also has a high heat rate. These high values at the top and bottom are due a lack of borated graphite holder shielding above and below the compact stack which allows thermal neutrons from the ATR driver fuel to leak into the top and bottom of the stacks and enhance the fission rate on these axial ends of the compact stack.

Radiation heat transfer using the ABAQUS *Gap Radiation model was implemented surface pairs.

Table 2. Capsule 5 base case compact heat rates

ABAQUS Element Group	Heat Rate (W/cm^3)
Stack2-Compact4-Top	79.26
Stack2-Compact4-Bot	65.84
Stack2-Compact3-Top	65.00
Stack2-Compact3-Bot	63.82
Stack2-Compact2-Top	65.59
Stack2-Compact2-Bot	67.38
Stack2-Compact1-Top	71.93
Stack2-Compact1-Bot	91.16
Stack1-Compact4-Top	86.04
Stack1-Compact4-Bot	74.51
Stack1-Compact3-Top	70.78
Stack1-Compact3-Bot	71.70
Stack1-Compact2-Top	72.80
Stack1-Compact2-Bot	74.04
Stack1-Compact1-Top	81.33
Stack1-Compact1-Bot	97.74
Stack3-Compact4-Top	54.95
Stack3-Compact4-Bot	40.09
Stack3-Compact3-Top	38.03
Stack3-Compact3-Bot	38.79
Stack3-Compact2-Top	39.00
Stack3-Compact2-Bot	40.49
Stack3-Compact1-Top	46.75
Stack3-Compact1-Bot	63.18

The control gas gap and the compact-graphite holder gas gaps were modeled as changing linearly with time. This was accomplished by having the gap conductivity of each capsule change with neutron fluence. Fluence was set as Field Variable 2 in the ABAQUS model. The original finite element mesh models created in ABAQUS were done with the as-built dimensions for the gas gaps. The gas gaps were assumed to be the hot gas gap dimension, the hot gas gap dimension and room temperature gas gap dimension being virtually the same. Experimental data obtained from the AGR-1 experiment were used for the compact and graphite shrinkage. This was done since the compacts are very closely related in properties in the two tests, and the borated graphite in AGR-1 Capsules 1 and 6 are nearly identical to the amount of B4C in AGR-2 capsules. Table 3 shows the Δr/r values obtained from measured values from the AGR-1 compact, holder holes, and graphite holder outside diameter as noted in [1]. These values take into account actual data measured for shrinkage of the compacts and graphite holder. Compact shrinkage values remain constant above a fluence of 3.0. Holder holes show a shrinkage rate of -0.23% per $1x10^{25}$ n/m^2 while the holder outside diameter is at -0.18%.

Table 3. Compact and graphite holder shrinkage as a function of fast neutron fluence.

Fast Fluence ($n/m^2 \times 10^{-25}$)	AGR-1 Compacts	Holder Holes	Holder OD
E > 0.18 MeV	actual Δr/r	Δr/r	Δr/r
0.0	0.0000	0.0000	0.0000
1.0	-0.0059	-0.0023	-0.0018
2.0	-0.0095	-0.0045	-0.0036
3.0	-0.0110	-0.0068	-0.0054
4.0	-0.0110	-0.0091	-0.0072
6.0	-0.0110	-0.0136	-0.0108
8.0	-0.0110	-0.0181	-0.0144

The top five parameters that can be quantified with an uncertainty are shown in Table 4 with the estimated value. All of these values are the best estimate of what the uncertainty is based on machining tolerances, physics code calculations, mass flow controllers, and engineering experience.

Table 4. Uncertainties of most significant parameters

Parameter	Uncertainty (%)
Control gas gap width	10
Heat rate in fuel compacts	5
Ne fraction	2-8
Graphite Conductivity	15

RESULTS

Results of this sensitivity analysis are shown in Figures 10 through 14. Figure 10 shows a cross-cut view of the temperature contours of the fuel compacts and graphite holder for the base case. The maximum fuel temperature is 1187°C. The maximum fuel temperature occurs in the fuel compacts near the center of the graphite holder.

Table 5 gives a description of the 27 cases that were run. The base case is taken as Case 0, while Cases 1 and 2 show the temperature change for changing the outer control gas gap distance by ±10%. This control gas gap was changed by multiplying the thermal conductivity of the control gas by 0.9 and 1.1 which provided the equivalent effect of moving the gap distance by ±10% respectively. This was a lot easier than making a geometrical change to the finite element mesh. Cases 3 and 4 show the temperature sensitivity by varying the neon fraction by ±10%. Other cases studied include fuel conductivity; graphite conductivity; compact-holder gap conductivity, emissivity of stainless steel, thru tubes, and graphite; and heat rate in compacts, graphite holder, and other capsule components. Cases 20 through 25 show the effect of fast neutron fluence varying from 0 to 5.0 x 10^{25} n/m^2. Cases 26 and 27 show the sensitivity of changing the control gas gap by ±20%. The base case peak compact temperature shown in Table 5 is 1206.80°C. Table 5 also

shows the resulting capsule average temperature, peak capsule temperature, thermocouple 1 (TC1), and TC2 temperatures. TC1 is at 307° clockwise rotation from north, while TC2 is at 233° as shown in Figure 2. The last four columns show the temperature difference in each of the cases compared to the base case for the average, peak, TC1, and TC2. The base case is highlighted in gold, while the peak fuel temperatures are highlighted in yellow.

Figure 11 shows a tornado plot of the peak fuel temperature variations sorted from largest to smallest caused by each 10% change in corresponding input parameters (except the top bar representing 20% change in outer control gap distance). Apparently, the control gap distance, heat rate in the compacts, and control gas fraction have the biggest effect on peak fuel temperature (or are the most sensitive parameters). The next four are heat rate in the graphite holder, graphite holder thermal conductivity, compact conductivity, and gas gap conductivity between compacts and graphite holder. The emissivities of the graphite and stainless steel, along with the heat rates in the components and emissivity of the thru tubes are the least sensitive. The total temperature sensitivity for ±20% outer control gap distance is 120.23°C, as displayed on the left side of the plot.

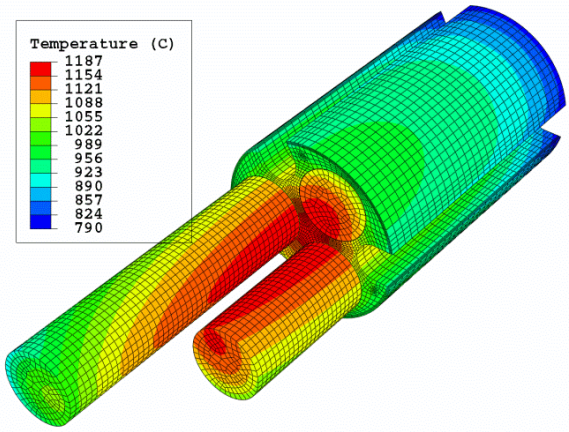

Figure 10. Temperature contour plot (°C) compacts and graphite holder

Table 5. Description of cases with temperature results in (°C)

Case #	Description	Capsule Average (°C)	Capsule Max (°C)	TC1 (°C)	TC2 (°C)	Δ Capsule Average (°C)	Δ Capsule Average (°C)	Δ TC1 (°C)	Δ TC2 (°C)
0	Base Case	1082.05	1206.80	952.07	891.81	0.00	0.00	0.00	0.00
1	1.1 X outer control gap distance	1115.80	1237.98	988.42	927.41	33.75	31.18	36.35	35.60
2	0.9 X outer control gap distance	1050.95	1178.03	918.54	859.10	-31.10	-28.77	-33.53	-32.71
3	1.1 X Ne fraction	1122.14	1245.76	989.67	928.61	40.09	38.96	37.60	36.80
4	0.9 X Ne fraction	1045.01	1170.65	917.35	857.98	-37.04	-36.15	-34.72	-33.83
5	1.1 X FUEL conductivity	1078.28	1197.69	951.59	891.88	-3.77	-9.11	-0.48	0.07
6	0.9 X FUEL conductivity	1086.61	1217.72	952.60	891.74	4.56	10.92	0.53	-0.07
7	1.1 X GRAPHITE (5.5% Boron) conductivity	1076.21	1197.81	949.31	890.34	-5.84	-8.99	-2.76	-1.47
8	0.9 X GRAPHITE (5.5% Boron) conductivity	1088.78	1217.02	955.28	893.58	6.73	10.22	3.21	1.77
9	1.1 X gap conductivity INT4 (holder/compact gap)	1077.36	1201.53	952.03	891.89	-4.69	-5.27	-0.04	0.08
10	0.9 X gap conductivity INT4 (holder/compact gap)	1087.58	1213.00	952.13	891.73	5.53	6.20	0.06	-0.08
11	1.1 X emissivity of SS retain	1077.15	1202.09	946.73	886.93	-4.90	-4.71	-5.34	-4.88
12	0.9 X emissivity of SS retain	1087.11	1211.67	957.59	896.85	5.06	4.87	5.52	5.04
13	0.9 X emissivity of graphite	1084.98	1209.88	954.34	893.88	2.93	3.08	2.27	2.07
14	1.1 X heat rate in fuel	1130.55	1263.97	989.30	926.68	48.50	57.17	37.23	34.87
15	0.9 X heat rate in fuel	1031.63	1147.42	913.28	855.57	-50.42	-59.38	-38.79	-36.24
16	1.1 X heat rate in graphite	1095.50	1220.77	966.60	905.28	13.45	13.97	14.53	13.47
17	0.9 X heat rate in graphite	1068.42	1192.64	937.34	878.18	-13.63	-14.16	-14.73	-13.63
18	1.1 X heat rate in components	1085.58	1210.21	955.94	895.44	3.53	3.41	3.87	3.63
19	0.9 X heat rate in components	1078.50	1203.38	948.19	888.16	-3.55	-3.42	-3.88	-3.65
20	0.0 fluence	1056.86	1173.18	939.73	884.29	-25.19	-33.62	-12.34	-7.52
21	0.001 fluence	1060.85	1178.93	941.53	884.93	-21.20	-27.87	-10.54	-6.88
22	0.01 fluence	1066.28	1186.52	944.09	886.05	-15.77	-20.28	-7.98	-5.76
23	0.1 fluence	1075.76	1198.81	948.83	889.05	-6.29	-7.99	-3.24	-2.76
24	1.0 fluence	1121.12	1250.70	970.99	907.87	39.07	43.90	18.92	16.06
25	5.0 fluence	1185.51	1311.59	1038.78	972.51	103.46	104.79	86.71	80.70
26	1.2 X outer control gap distance	1152.48	1271.65	1027.90	966.18	70.43	64.85	75.83	74.37
27	0.8 X outer control gap distance	1022.20	1151.42	887.48	828.99	-59.85	-55.38	-64.59	-62.82

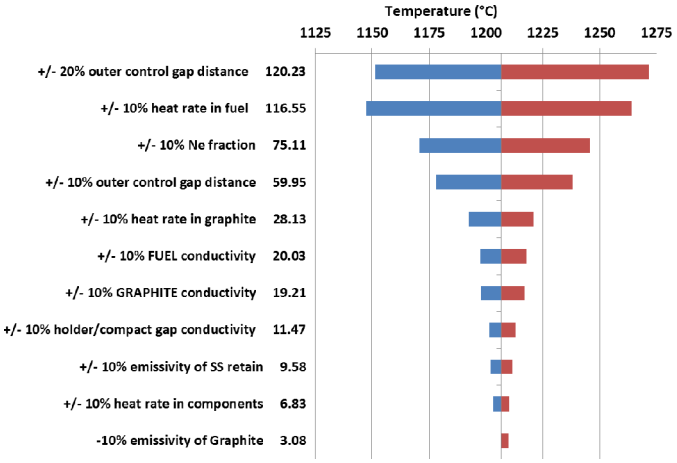

Figure 11. Tornado plot of peak fuel temperature sensitivity (base case = 1206.80°C).

Figures 12 and 13 show tornado plots for the temperature sensitivity for TC1 and capsule average temperature, respectively. The order of the sensitivity remains the same for all three plots for the top five parameters. TC1 temperature is more sensitive to the emissivity in the thru tubes since the TC1 is in close proximity.

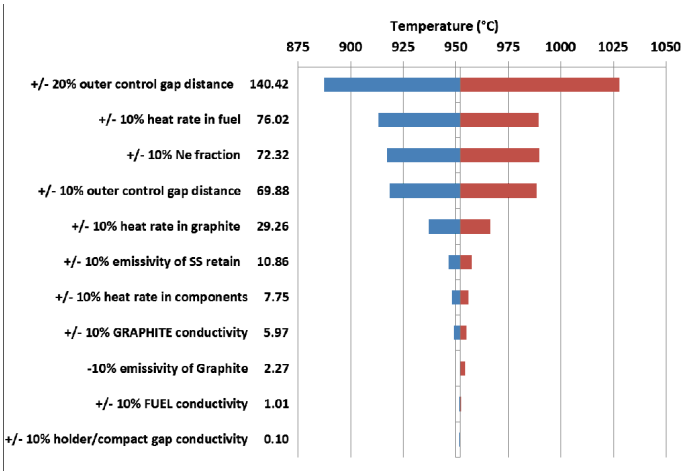

Figure 12. Tornado plot of TC1 temperature sensitivity (base case = 952.07°C)

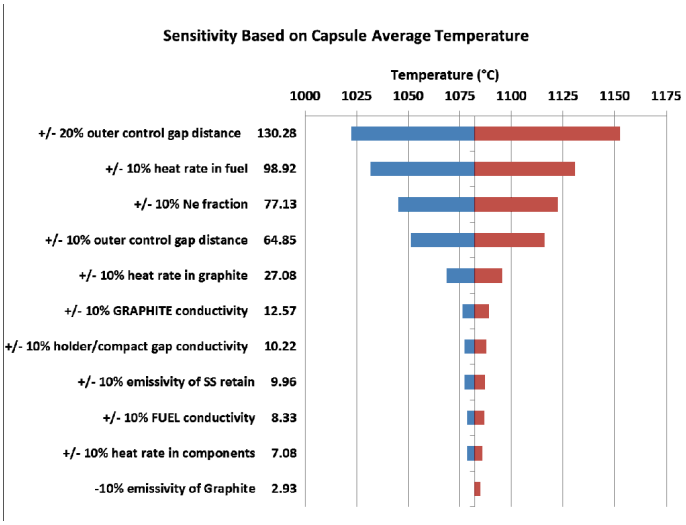

Figure 13. Tornado plot of capsule average temperature sensitivity (base case = 1082.05°C)

Figure 14 shows the peak fuel temperature sensitivity as a function of fast neutron fluence. The fluence values have an effect on the thermal conductivity of the fuel compacts and the graphite components. As mentioned above, the gas gaps change size based on the graphite holder shrinking due to neutron damage. Figure 14 shows that a fluence of 0.0 is 33°C cooler than the base case at a fluence of 0.23, while a fluence value of 5.0 is 105°C hotter.

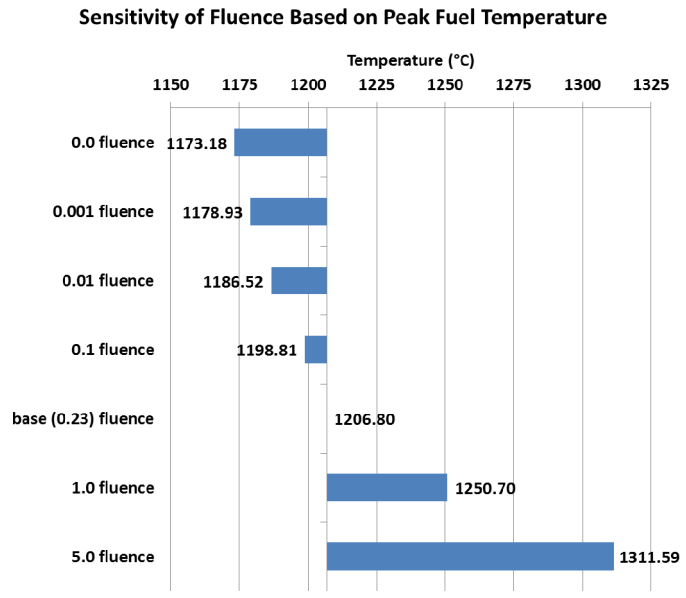

Figure 14. Plot of peak fuel temperature sensitivity based on fluence (base case = 1206.80°C)

The variable gap model includes the graphite holder shrinking and the gas gap between the holder and stainless steel retainer growing, thus causing the large temperature change.

This is a result of the control gas gap becoming larger due to the graphite holder shrinkage with neutron damage. A smaller sensitivity is due to the thermal conductivity of the fuel compacts and graphite holder decreasing with fast neutron fluence.

CONCLUSIONS

A temperature sensitivity evaluation has been performed for the AGR-2 fuel experiment on an individual capsule. A series of cases were compared to a base case by varying different input parameters into the ABAQUS finite element thermal model. These input parameters were varied by ±10% to evaluate the temperature sensitivity variation of each parameter. The most sensitive parameters were the outer control gap distance, heat rate in the fuel compacts, and neon gas fraction. Thermal conductivity of the compacts and graphite holder exhibited moderate sensitivity. The smallest sensitivities were for the emissivities of the stainless steel, graphite, and thru tubes. Sensitivity calculations were also performed varying with fluence. These calculations showed a general temperature rise with an increase in fluence. This is a result of the variable gas gap model implemented where the graphite holder shrinks and the gas gap grows with an increase in fluence. The thermal conductivity of the fuel compacts and graphite holder vary with fluence, causing a temperature increase as fluence increases.

NOMENCLATURE

A radiation surface area (m^2)
dpa displacements per atom
F_{12} view factor from surface 1 to 2 k
thermal conductivity (W/m-K) MeV
million electron volts
MW molecular weight
Q volumetric heat rate (W/m^3)
T temperature, °C
x,y,z Cartesian coordinates (m)

Greek Letters

Γ fast neutron fluence (n/m^2)
μ molecular viscosity (kg/m-s)
σ Stefan-Boltzmann constant (W/m^2-K^4)
ε emissivity

Subscripts

DNE dido nickel equivalent
irr irradiated
0 unirradiated

ACKNOWLEDGMENTS

Work supported by the U.S. Department of Energy, NGNP Program, Idaho Operations Office Contract DE-AC07-05ID14517.

REFERENCES

[1] G. L. Hawkes, et. al., "Thermal Predictions of the AGR-2 Experiment with Variable Gas Gaps," paper # 10218, ANS Summer Meeting, Reno, NV June 2014.

[2] Dassault Systèmes, ABAQUS Version 6.9-2, www.simulia.com or www.abaqus.com, Providence, Rhode Island, 2009.

[3] R. Gontard and H. Nabielek, "Performance Evaluation of Modern HTR TRISO Fuels," Forschungszentrum Jülich GmbH, HTA-IB-05/90, July 31, 1990.

[4] T. L. Albers, Letter from GrafTech to the Idaho National Laboratory, October 5, 2009.

[5] L. L. Snead and T. D. Burchell, "Reduction in Thermal Conductivity Due to Neutron Irradiation, 22nd Biennial Conference on Carbon, Extended Abstracts 774-775 (1995).

[6] J. W. Sterbentz, "Fast Flux to DPA Multiplier," E-mail communication to G.L. Hawkes, August 5, 2009.

[7] Fluent Inc., "Fluent 6.3 User's Guide," Lebanon, NH, September 2006.

[8] Y. S. Touloukian, "Thermophysical Properties of Matter, Volume 3 – Thermal Conductivity," Thermophysical Properties Research Center, Purdue University, 1977.

[9] J.W. Sterbentz, "JMOCUP As-Run Daily Depletion Calculation for the AGR-2 Experiment In the Advanced Test Reactor B-12 Position," ECAR-2066, Rev. 2, Idaho National Laboratory, April 2014.